Probabilistic atlas of the C57BL/6J mouse cerebellum

Jeremy F.P. Ullmann[b], Andrew Janke[b], Charles Watson[a, c], Nyoman D. Kurniawan[b], George Paxinos[a, d], Marianne D. Keller[b], Zhengyi Yang[b], Kay Richards[h], Gary F. Egan[a, g], Steven Petrou[a, h, i], Graham J. Galloway[a, b], and David C. Reutens[a, b]

[a] The Australian Mouse Brain Mapping Consortium, The University of Queensland, Australia. [b] The Centre for Advanced Imaging , The University of Queensland, Australia. [c] Health Sciences, Curtin University, Australia. [d] Neuroscience Research Australia, The University of New South Wales, Australia. [e] The Queensland Brain Institute, The University of Queensland, Australia. [f] Faculty of Medicine, Nursing and Health Sciences, Monash University, Australia. [g] Monash Biomedical Imaging, Monash University, Australia. [h] Florey Neuroscience Institutes, Australia. [i] Centre for Neuroscience, The University of Melbourne, Australia.

The University of Queensland, Australia
Centre for Advanced Imaging
Australian Mouse Brain Mapping Consortium

Introduction

The cerebellum is involved in motor control and cognitive functions and is affected by numerous neurological diseases. The anatomy of the mouse cerebellum is well characterized and depicted in detailed paper-based atlases which use cytoarchitectural features to establish structural delineations in individual brains. More recently, magnetic resonance imaging (MRI), which permits the registration of multiple data sets, has been used to create digital atlases and assess anatomical variabiltiy. Existing MRI-based atlases contain a limited segmented cerebellar structures, limiting the level at which statistical and computational comparisons between individuals or groups can be performed. In this study we developed 1) a detailed protocol for segmenting the *ex vivo* C57BL/6J cerebellum on high-resolution MR images and 2) a probabilistic atlas of the C57BL/6J cerebellum.

Methods

18 animals were perfused and fixed with 4% paraformaldehyde and 0.1% Magnevist®. Brains were extracted and incubated in 0.1% Magnevist/ PB for 4 days, placed in Fomblin and imaged on a 16.4T (89mm) Bruker micro-imaging system using a 15 mm SAW coil. MRI data were acquired using a 3D gradient echo sequence with TR/TE/FA= 50ms/12ms/30°, 82 KHz spectral bandwidth, and 8 excitations with an acquisition time of 5h 15mins to produce T_1/T_2^*-weighted images at 30µm³ isotropic resolution.

Images were placed in the stereotaxic Waxholm space and a symmetric model was created using a recursive non-linear hierarchical fitting strategy. The final fitting step used a nonlinear transformation with a step size of 30µm. This resulted in a model with double the resolution of the original input data (15µm vs. 30µm).

The components of the cerebellum were then delineated, on the bases of differences in signal intensity and/or their location in reference to cerebral fissures, and partitioned using vector-based segmentation via a Cintiq tablet. Subsequently, surface smoothed three-dimensional surface reconstructions were created in Amira.

A probabilistic model was created using the same method as the ICBM152 model. Namely the traced structures were nonlinearly transformed back to native space before a lower order nonlinear native space to model space transform was applied. In our case this was a grid transform with a step size of 4 times that of the voxel size (60um).

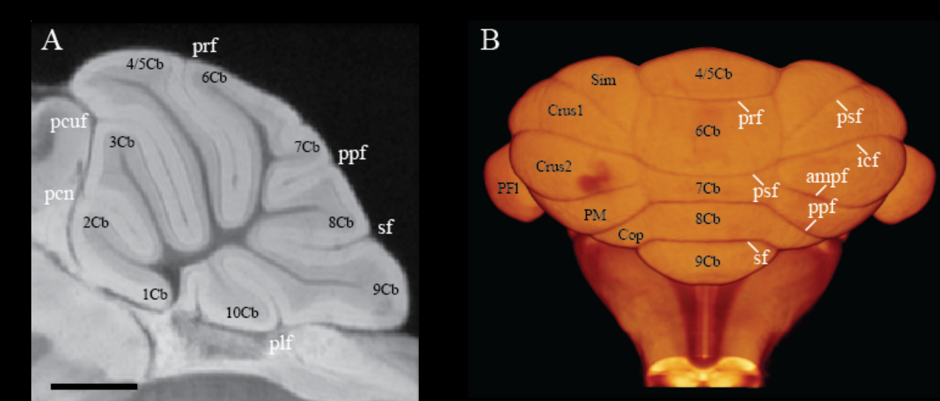

Fig. 1. The lobules and folial pattern of the C57BL/6J cerebellum. (A) Midsagittal section of the cerebellum, scale bar = 1 mm. (B) Surface renderings of the cerebellum. Cerebellar regions are in black and fissures and sulci are in white.

Structure	Abbreviation	Color Code	Average Volume (mm^3)	Average Signal Intensity (%)
Lobules of cerebellar vermis				
Lobule 1	1Cb		0.14	83.5
Lobule 2	2Cb		1.16	84.3
Lobule 3	3Cb		1.79	78.8
Lobules 4/5	4/5Cb		5.61	78.1
Lobule 6	6Cb		2.50	74.9
Lobule 7	7Cb		0.67	75.2
Lobule 8	8Cb		1.52	75.2
Lobule 9	9Cb		2.81	78.7
Lobule 10	10Cb		1.26	86.7
Lobules of cerebellar hemispheres				
Simple lobule	Sim		4.67	78.4
Crus 1 of the ansiform lobule	Crus 1		4.17	74.6
Crus 2 of the ansiform lobule	Crus 2		4.18	74.6
Paramedian lobule	PM		3.59	76.4
Copula of the pyramis	Cop		2.00	79.7
Paraflocculus	PFl		3.35	72.1
Flocculus	Fl		0.79	79.6
Cerebellar, vestibular, and cochlear nuclei				
Lateral cerebellar nucleus	Lat		0.35	65.2
Lateral cerebellar nucleus, parvicellular part	LatPC		0.05	68.9
Medial cerebellar nucleus	Med		0.28	57.4
Medial cerebellar nucleus, lateral part	MedL		0.02	62.5
Medial cerebellar nucleus, dorsolateral protuberance	MedDL		0.11	60.6
Interposed cerebellar nucleus, anterior	IntA		0.32	60.9
Interposed cerebellar nucleus, posterior	IntP		0.22	62.8
Interposed cerebellar nucleus, posterior parvicellular part	IntPPC		0.04	71.8
Interposed cerebellar nucleus, dorsolateral hump	IntDL		0.10	61.7
Dorsal cochlear nuclei	DC		0.54	77.5
Ventral cochlear nuclei, anterior part	VCA		0.18	70.0
Ventral cochlear nuclei, posterior part	VCP		0.44	66.9
Cerebellar white matter				
Superior cerebellar peduncle	scp		0.25	55.2
Decussation of the superior cerebellar peduncle	xscp		0.09	62.4
Middle cerebellar peduncle	mcp		1.52	47.2
Inferior cerebellar peduncle	icp		0.28	46.7
Other structures				
Dorsal acoustic stria	das		0.03	43.0
Superior medullary velum	SMV		0.04	86.8
Ventral spinocerebellar tract	vsc		0.01	49.3

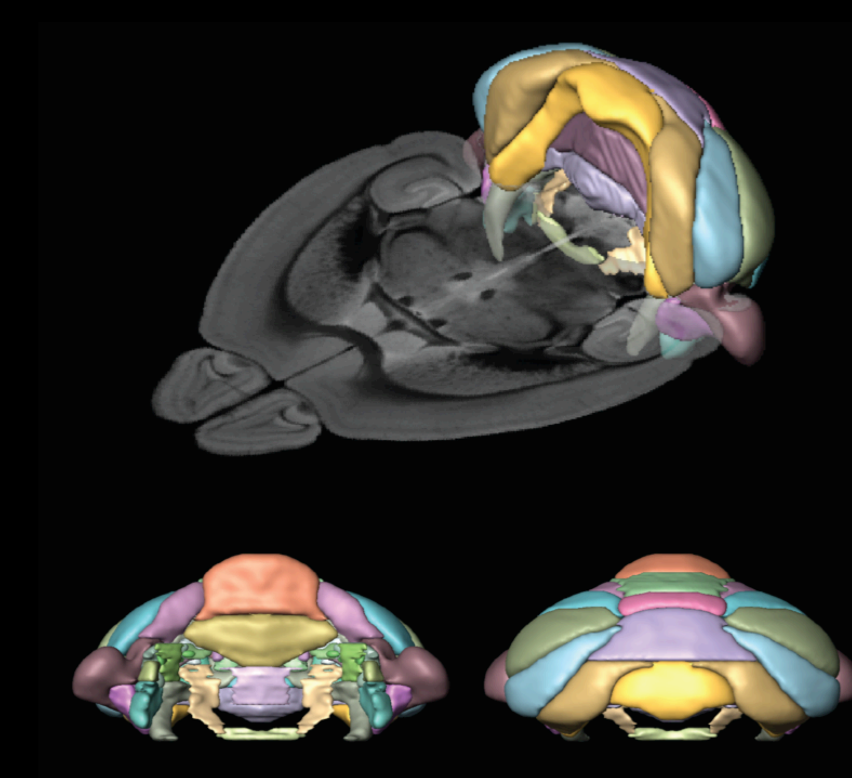

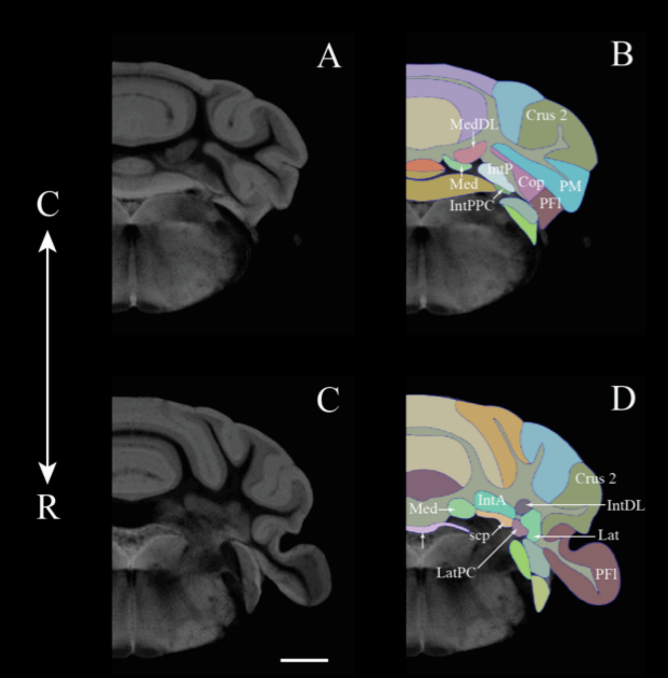

Fig. 2. Segmentation of the central region of the cerebellum. Coronal views of T_2^* average image (A, C) and corresponding segmented image (B, D). R-C denotes rostral-caudal direction.

Fig, 5. Probabilistic volumes for the C57BL/6J cerebellum. A probability of 1 (100%) means that all individual segmentations on 18 brains overlap on a given voxel. Some areas with the greatest variability are indicated with arrows. Slice positions are given in Waxholm space. Scale bar = 1 mm.

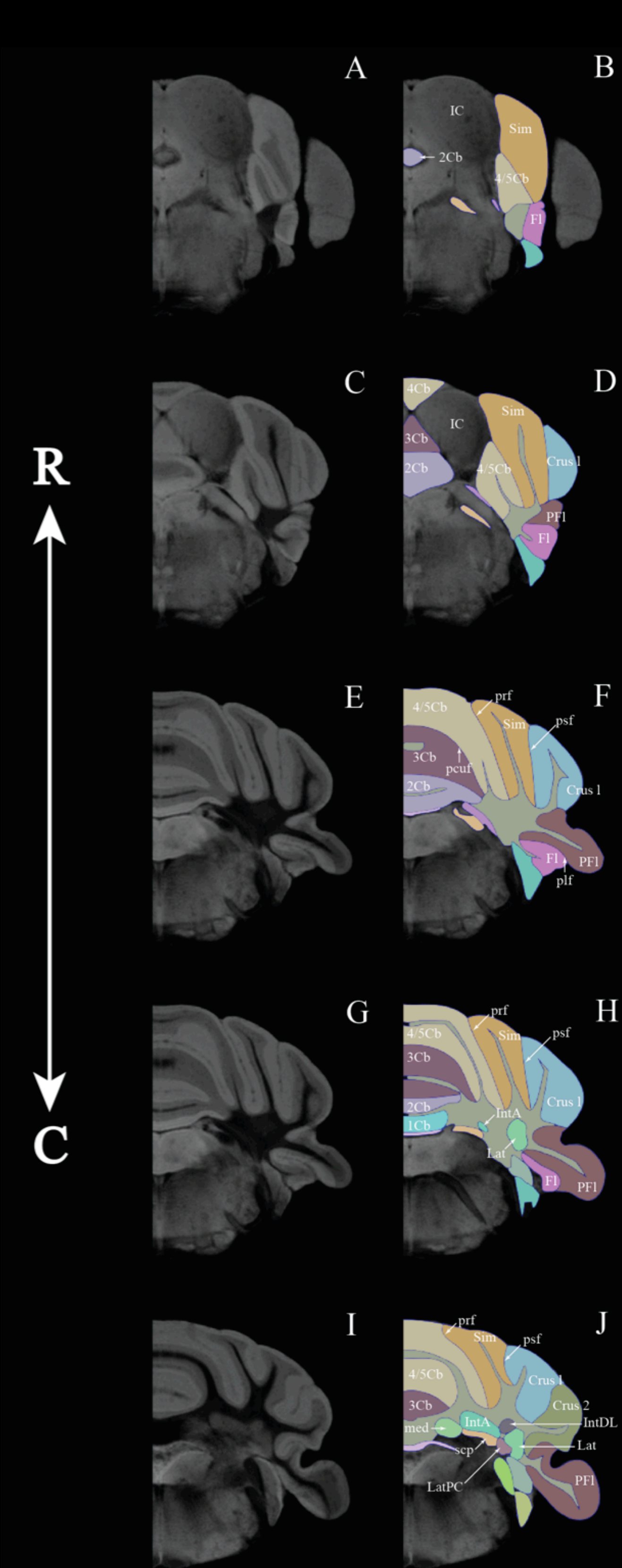

Fig. 3. Segmentation of the caudal vermis and the copula and paramedial lobule. Representative T_2^* average images (A, C, E, G, I) and corresponding segmented image (B, D, F, H, I). R-C denotes rostral-caudal direction and dashed lines indicate manually delineations required for MRI-based segmentation.

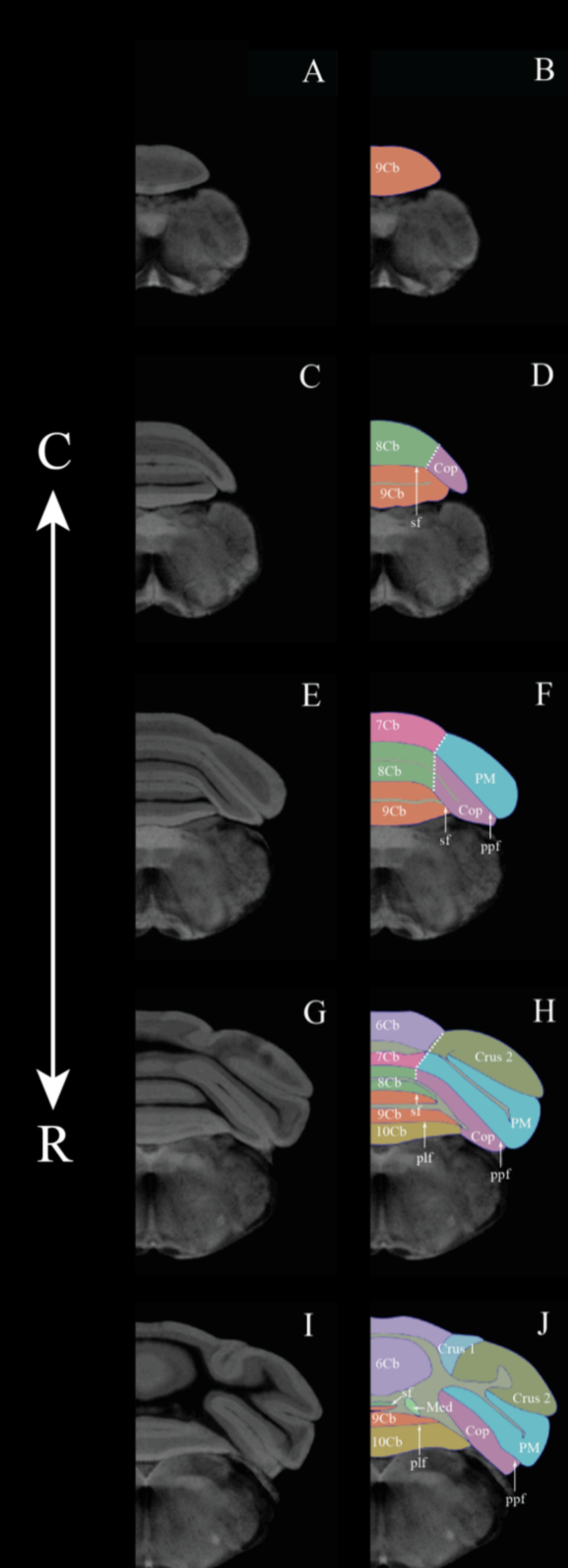

Fig. 4. Segmentation of the central region of the cerebellum. Coronal views of T_2^* average image (A, C) and corresponding segmented image (B, D). R-C denotes rostral-caudal direction.

Results & Conclusion

- Established a protocol for for systematic delineation of the C57BL/6J mouse cerebellum in magnetic resonance images.
- The key to cerebellar segmentation is the identification of the fissures. The fissures separate the major vermal lobules and the parts of the cerebellar hemispheres (Fig.1).
- Delineated 38 cerebellar and cerebellar-related structures (Fig. 2,3,4).
- Calculated average region volumes and average T_2^* intensities for each structure (Table 1).
- Created probabilistic maps for each structure (Fig. 5).
- The atlas will assist the segmentation of the cerebellum of novel mutants with C57BL/6J backgrounds and will permit the identification of altered morphologies.